Electrochemical Impedance Spectroscopy Investigations of a Microelectrode Behavior in a Thin-Layer Cell: Experimental and Theoretical Studies

C. Gabrielli, M. Keddam, N. Portail, P. Rousseau, H. Takenouti, and V. Vivier*

UPR 15 du CNRS, Laboratoire Interfaces et Systèmes Electrochimiques, Université Pierre et Marie Curie, 4, place Jussieu, case courrier 133, 75252 Paris, Cedex 05, France

Received: May 18, 2006; In Final Form: July 27, 2006

Electrochemical impedance spectroscopy experiments were performed on a microdisk electrode in a thin-layer cell using a scanning electrochemical microscope for controlling the cell geometry. Experimental data showed that when the thin-layer thickness diminished, an additional low-frequency response appeared. It was ascribed to the radial diffusion of the electroactive species and was strongly dependent on the thin-layer dimensions (both thickness and diameter). Moreover, the numerical simulation of the impedance diagrams by finite element method calculations confirmed this behavior. An equivalent circuit based on a Randles-type circuit was proposed. Thus, the diffusion was described by introducing two electrical elements: one for the spherical diffusion and the other for the radial contribution. A nonlinear Simplex algorithm was used, and this circuit was shown to fit the impedance diagrams with a good accuracy.

Introduction

Microelectrodes, which are usually called ultramicroelectrodes (UME) when they are in the micrometer range, were widely developed in the last 30 years mainly because of the advantages in electroanalytical chemistry.[1−8] The most common microelectrode is the microdisk electrode that easily can be made by sealing a small diameter wire in an insulator.[9] Because of their small size (at least one of the dimensions is in the micrometer range), these electrodes have numerous advantages compared to electrodes of conventional size, that is, the diffusional mass transport is very efficient even in the absence of convection. They also have many other typical and attractive characteristics. Among these characteristics are the establishment of a steady-state current, I_∞, which is proportional to the electrode radius a[7] and a greatly reduced double-layer capacitance caused by the small active area dimension that results in a small RC time constant, which allows high-speed cyclic voltammetry to be performed.[7−9]

Electrochemical impedance spectroscopy (EIS) has been widely recognized as a powerful tool for the investigation of electrochemical systems.[10,11] Although there is interest in this technique, only a few papers have dealt with the combined use of EIS and microelectrodes.[12−27] Thomas and Brodd[12] reported the determination of the diffusion coefficient of the iodine−iodide oxidation−reduction couple using faradaic impedance measurements at platinum microelectrodes. McNaughtan et al.[17] developed an experimental setup for large impedance measurements suitable for use with UME. Baranski et al.[18,19] developed high-frequency impedance measurements (up to 5 MHz), which enabled the studies of very fast surface processes. Aoki and Tokida[22] used the high-frequency part of the impedance to determine the resistance of HCl solutions without any supporting electrolyte. Dexter and co-workers[26] reported the use of Au−Hg microelectrodes with EIS to distinguish between the electrochemical response of one- and two-electron-transfer reactions within a marine microbial biofilm. In addition, valuable information on charge transfer occurring at the electrode may be obtained. For instance, Koehler and Bund[27] investigated the kinetics of electron-transfer reactions in magnetic fields for some iridium and iron complexes. From cyclic voltammetry, linear sweep voltammetry, and EIS measurements, they showed that a magnetic field up to 1 T had no influence on the rate of the electron transfer. Vivier et al.[23,28] used EIS measurements to characterize the electrochemical behavior of electroactive powder inserted in a cavity microelectrode. Isaacs et al.[29] reported the use of a pair of microelectrodes for the measurements of local ac currents which allows a local impedance to be determined.

Several groups focused their attention on the high-frequency part of the electrochemical impedance to evaluate the electrolyte resistance.[24,30−34] Coupled with the scanning electrochemical microscope, this measurement was shown to have a good spatial resolution[24,31,34] and was successfully applied to the in situ characterization of the dendrite formation between two copper microwire in oxalic acid solutions.[31]

In the same way, many theoretical works have dealt with the calculation and the simulations of various electrochemical techniques involving microelectrodes.[5,7,15,21,35−41] For an ideal impedance measurement, Fleischmann et al.[5,15] established semianalytical relations for the diffusion part Z_d of the impedance Z. They have shown that Z_d is the solution of a Bessel-type differential equation and can be expressed as

$$\mathrm{Re}(Z_d) = \frac{4RT}{\pi n^2 F^2 \sqrt{D\omega} a^2 c^\infty} \Phi_4\left(\frac{a^2\omega}{D}\right) \quad (1)$$

$$-\mathrm{Im}(Z_d) = \frac{4RT}{\pi n^2 F^2 \sqrt{D\omega} a^2 c^\infty} \Phi_5\left(\frac{a^2\omega}{D}\right) \quad (2)$$

where $\mathrm{Re}(Z_d)$ and $\mathrm{Im}(Z_d)$ are the real and imaginary parts of Z_d, respectively, R is the gas constant, T is the temperature, and Φ_4 and Φ_5 are tabulated functions in ref 5. The ratio ($a^2\omega/D$) represents a dimensionless frequency. These equations have

* Corresponding author. E-mail: vivivier@ccr.jussieu.fr. Tel: 33 1 44 27 41 58. Fax: 33 1 44 27 40 74.

10.1021/jp063055h CCC: $33.50
Published on Web 09/16/2006

been corroborated by experimental works.[16,17,24] Ferrigno and Girault[21] used a finite element method (FEM) to calculate the impedance of microdisk electrodes. However, because of the software used, they were limited to recessed microdisk geometries to avoid any flux discontinuity at the electrode edge.

Finally, although the thin-layer-cell theory was devised a few decades ago because of the pioneering works of Hubard and Anson,[42−44] no attention has been paid to the description of electrochemical impedance measurements on microelectrodes in a thin-layer configuration. This situation is of interest because it corresponds to practical cases such as the study of pitting corrosion or the electrochemical characterization of individual entities such as biological cells.

The primary objectives of this paper are the description, the interpretation, and the simulation of EIS measurements on microdisk electrodes in a thin-layer cell. This configuration was achieved by using a scanning electrochemical microscope (SECM)[45−53] in negative feedback mode and by taking the $Fe(CN)_6^{3-}/Fe(CN)_6^{4-}$ redox couple as an example.

Experimental Section

The thin-layer-cell experiments were performed with a homemade SECM apparatus.[24,50,51] It consisted of a 3-axis positioning system (VP-25XA, Newport) driven by a motion encoder (ESP300, Newport) that allowed a spatial resolution of 100 nm in the three directions. The electrochemical measurements were carried out with a homemade bipotentiostat coupled to a low-noise current-to-voltage converter (Femto DLPCA200, BFI Optilas) with an adjustable gain (10^3-10^{11} V/A) and a large bandwidth (up to 500 kHz). This experimental setup allowed electrochemical impedance spectroscopy to be performed on microelectrodes (the difficulties of large impedance measurements especially in the high-frequency domain were already reported[24] and will not be rediscussed here). The frequency response analyzer was a Solartron 1250. All measurements were performed under a potentiostatic regulation with a 30 mV peak-to-peak signal, 20 acquisition cycles, and 7 points per decade of frequency. Software made in-house and developed under Labview environment was used for data acquisition.

SECM tips consisted of homemade platinum microelectrodes that were 5 or 10 μm in radius with platinum wires sealed into soft glass. The normalized radius of the UME in which $RG = r_g/a$ (a and r_g are the radii of the platinum wire and the tip-insulating material, respectively) was set between 10 and 20 and was determined by both scanning electron microscope (SEM) observation and by recording an approach curve at an insulating substrate. Potentials were measured with respect to a saturated calomel electrode (SCE), and the counter electrode was a 0.5 cm^2 platinum grid. Before each experiment, UME was cycled for a few minutes at scan rates higher than 1 V s^{-1} in a 0.5 M H_2SO_4 solution to ensure a perfect cleaning. Then, cyclic voltammetry experiments were performed in a 0.01 M $K_4Fe(CN)_6$ + 0.01 M $K_3Fe(CN)_6$ + 0.5 M KCl solution at 10 mV s^{-1} to evaluate the experimental steady-state current and to compare it to the theoretical value determined from the formula[7] $I_\infty = 4nFDc^\infty a$ (n is the number of exchanged electrons, F is the Faraday constant, D is the diffusion coefficient, and c^∞ is the bulk concentration of the electroactive species). All impedance experiments were performed with the same electrolytic solution as for cyclic voltammetry (CV) experiments.

All solutions were prepared in deionized and doubly distilled water from analytical-grade chemicals. ($K_3Fe(CN)_6/K_4Fe(CN)_6$) was purchased from SIGMA and used as received. KCl was used as a supporting electrolyte. Because the compound $K_3Fe(CN)_6/K_4Fe(CN)_6$ tends to form Prussian Blue, which adsorbs at the electrode surface, all solutions were freshly prepared.

Theory

Let us consider a simple reaction scheme such as

$$\mathrm{Ox} + e^- \underset{k_b}{\overset{k_f}{\rightleftharpoons}} \mathrm{Red} \tag{3}$$

where k_f and k_b are the rate constants for reduction and oxidation, respectively.

When a small ac amplitude perturbation is superimposed onto the dc component, the electrochemical impedance of the system is thus defined as

$$Z = \frac{\Delta\tilde{E}(\omega)}{\Delta\tilde{I}(\omega)} \tag{4}$$

where $\Delta\tilde{E}(\omega)$ and $\Delta\tilde{I}(\omega)$ are the potential and the current, respectively, and ω is the angular frequency. In the presence of a supporting electrolyte, migration effects can be neglected. If the electrochemical cell is assumed to be convection free during the experiment, the relation between the concentration perturbation Δc_i and the flux of matter at the electrode is given with a good approximation by the second Fick's law[10]

$$\frac{\partial \Delta c_i}{\partial t} = \nabla[D_i \nabla(\Delta c_i)] \tag{5}$$

D_i is a constant and by the use of the cylindrical coordinates, it can be expressed as

$$\frac{\partial \Delta c_i}{\partial t} = D_i\left(\frac{\partial^2 \Delta c_i}{\partial r^2} + \frac{1}{r}\frac{\partial \Delta c_i}{\partial r} + \frac{\partial^2 \Delta c_i}{\partial z^2}\right) \tag{6}$$

in which r is the radial coordinate measured from the center of the electrode and z is the normal coordinate to the electrode surface.

In the frequency domain, the Fick's law can be rewritten as

$$j\omega\, \Delta\tilde{c}_i = D_i\left(\frac{\partial^2 \Delta\tilde{c}_i}{\partial r^2} + \frac{1}{r}\frac{\partial \Delta\tilde{c}_i}{\partial r} + \frac{\partial^2 \Delta\tilde{c}_i}{\partial z^2}\right) \tag{7}$$

Girault et al.[21] used a Dirichlet boundary condition for $\Delta\tilde{c}_i/\tilde{c}_i$ (i.e., a constant concentration at the electrode surface), and Fleischmann et al.[15] used a Neumann boundary condition i.e., a constant flux at the electrode surface. However, a more rigorous treatment is necessary to use the Robin boundary conditions determined from the linearization of the Buttler−Volmer current−potential characteristic. With the boundary conditions for ΔE being a normalized potential perturbation at the surface of the electrode and a null value at the boundary corresponding to the bulk solution, the diffusional impedance is then obtained in a dimensionless form. The diffusional impedance is thus proportional to the reciprocal current−density integral on the electrode surface (complex quantity) through the following relationship

$$Z_d(\omega) = \frac{1}{nF}\frac{\Delta E \pi a^2}{2\pi D_i \int_0^a \left(\frac{\partial \Delta\tilde{c}_i}{\partial z}\right)_{z=0} r\,dr} \tag{8}$$

A Randles-type equivalent circuit is used to describe the electrochemical interface,[10] so the overall impedance Z is given by

$$Z(\omega) = R_e + \frac{1}{\frac{1}{Z_d(\omega) + R_{ct}} + jC_{dl}\omega} \quad (9)$$

in which R_e is the electrolyte resistance, C_{dl} is the double-layer capacitance, and R_{ct} is the charge-transfer resistance. In a previous paper,[24] we showed that the R_e evaluated from impedance measurements on a microdisk electrode in the high-frequency range was in good agreement with the predicted value from the Newman formula[54]

$$R_e = \frac{1}{4\kappa a} \quad (10)$$

where κ is the electrolyte conductivity.

The R_{ct} value is a direct measurement of the standard rate constant k^0 (which is directly linked to k_f and k_b [9]) of the electrochemical reaction through the relationship

$$k^0 = \frac{RT}{n^2F^2}\frac{1}{R_{ct}c^\infty} \quad (11)$$

In the high-frequency range, the diffusion impedance Z_d and the charge-transfer resistance can be neglected, so that the overall impedance depends on R_e and C_{dl} only, whereas in the low-frequency domain, the diffusional impedance predominates.

Finally, numerical calculations were performed using dimensionless quantities, but all the results presented in this paper will be given in dimension form to allow simpler comparisons with the experimental data. The boundary position in the bulk solution was chosen to ensure a relative error of less than 1% for all calculations.

Results

The thin layer was achieved using the SECM in the negative feedback mode as shown in Figure 1a. In an initial step, the tip electrode was brought close to the flat insulating substrate (a microscope glass slide) recording an approach curve at the approaching rate v_z of 1 μm s^{-1} (Figure 1b). The curve of Figure 1b was plotted using the usual SECM conventions (i.e., the normalized current I_{Norm} with respect to the normalized distance L). L and I_{Norm} represent the ratios d/a and I/I_∞, respectively, where d is the tip-to-substrate distance. The numerical simulation of the approaching curve (open circle in Figure 1b) by FEM calculations allowed a RG value of 18 to be determined. This value was consistent with SEM observations of the apex of the UME. This curve also allowed the tip to be positioned at a given distance of the substrate. Moreover, the point of contact between the tip and the microscope glass slide was evidenced by a significant change of the slope on the approach curve. In Figure 1b, this point is located at $L = 0.08$ and $I_{Norm} = 0.1$. Assuming that (i) the edge of the insulating part of the electrode was the point of contact between the tip and the substrate, and (ii) the surface roughness of the tip was negligible, the center of the electrode was at about 800 nm from the substrate. The tilt angle, β, between the microelectrode and the substrate is thus defined by

$$\sin\beta = L/RG \quad (12)$$

allowing an angle value of about 0.005 rad to be determined.

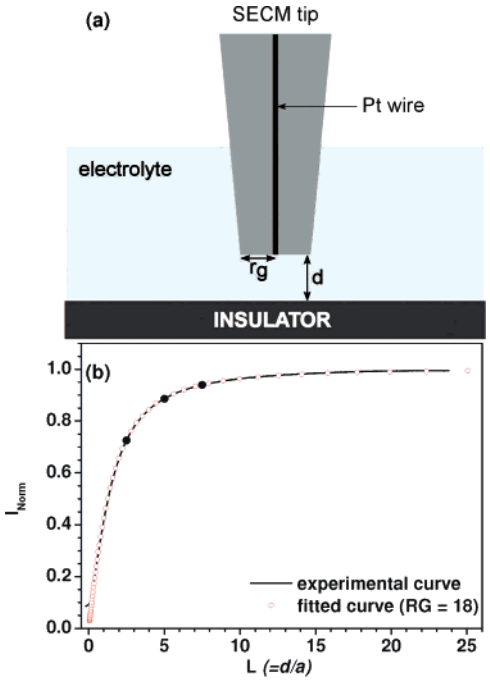

Figure 1. (a) Representation of the thin-layer geometry achieved with the SECM setup in negative feedback mode and (b) experimental (v = 1 μm s^{-1}) and calculated approaching curves.

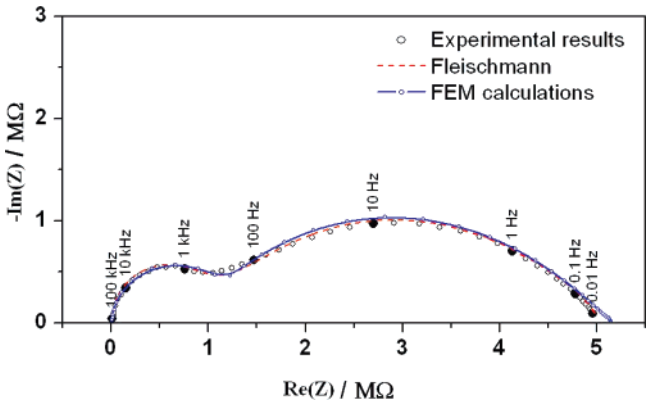

Figure 2. Impedance diagram recorded with a 10-μm-diameter Pt-microelectrode in a 10 mM $K_3Fe(CN)_6$ + 10 mM $K_4Fe(CN)_6$ + 0.5 M KCl solution at the equilibrium potential. Symbols, experimental data; dotted line, numerical simulations using Fleischmann et al. expression; and solid line, FEM simulations.

Thus, in a first approximation, the electrode was considered to be parallel to the substrate, and, thus, the formed thin layer was considered to be a right-circular cylinder having a base radius of RG and a height of L in dimensionless units.

Figure 2 shows a typical impedance diagram (Nyquist representation) of a 10-μm-diameter Pt-UME in a 10 mM $K_3Fe(CN)_6$ + 10 mM $K_4Fe(CN)_6$ + 0.5 M KCl solution measured at the equilibrium potential in the 0.01 Hz to 100 kHz range. This diagram was obtained in the bulk solution with no insulator facing the microelectrode tip. The high-frequency loop was ascribed to the electron-transfer process. At 100 kHz, the impedance was reduced to the electrolyte resistance R_e = 9.2 kΩ, which is in good agreement with the 9 kΩ value calculated with eq 10. The charge-transfer resistance was estimated to be R_{ct} = 1.2 MΩ. The value of the kinetic constant k^0 of the electron transfer, which was determined to be 2.5 $\times$ 10^{-2} cm s^{-1} according to eq 11, is in the range of the observed value.[55,56] This rate constant remained unchanged during each set of experiments showing that no electrode passivation based on

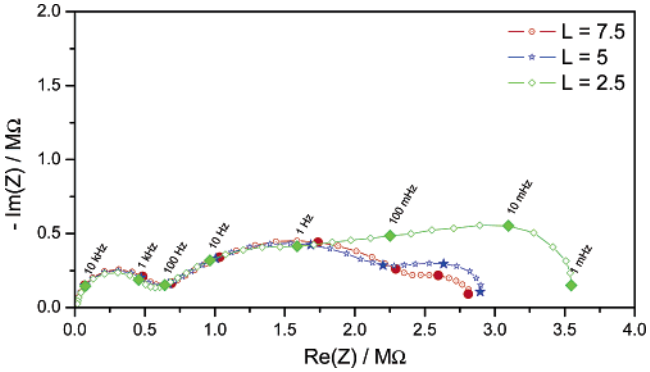

Figure 3. Experimental impedance diagrams of a Pt-microelectrode (20 μm-diameter) in a thin-layer cell with the dimensionless distance L as a parameter. Pt-microelectrode in a 10 mM $K_3Fe(CN)_6$ + 10 mM $K_4Fe(CN)_6$ + 0.5 M KCl solution.

$Fe(CN)_6^{3-/4-}$ decomposition to a Prussian blue-like film was observed. The value of the double-layer capacitance was ca. 41 pF (52 μF cm^{-2}), which is a common value for a platinum electrode. Because the frequency dispersion was rather small, it was neglected, and the double-layer capacitance was estimated from the characteristic frequency of a usual *RC* time constant. However, this contribution can be slightly different from one set of experiments to the other because C_{dl} depends on the state of the platinum surface of the UME.

The low-frequency loop was ascribed to the diffusion of the electroactive species in the solution. In contrast to the situation with electrodes of conventional sizes, the flux at the microelectrode reached a nonzero steady-state value, which was expressed by an impedance diagram that approaches the real axis at low frequencies.[5,16] As shown in Figure 2, a very good agreement was found between the experimental curve (circle) and the impedance curves numerically simulated from eqs 1−2 (Fleischmann et al. expressions, dotted line) or from eq 9 using FEM calculations (solid line) that validates both impedance measurements and simulations. From numerical simulations, the diffusion coefficient of the reactive species was found to be 6.60×10^{-6} cm^2 s^{-1}, which is in good agreement with that determined by cyclic voltammetry at 10 mV s^{-1} (6.45×10^{-6} cm^2 s^{-1}) and with those reported in the literature.[57]

Experimental impedance diagrams, which were recorded with a 20-μm-diameter Pt-microelectrode (RG = 18) in thin-layer cell with various thickness, are plotted in Figure 3. The electrolyte resistance increases as L decreases (not visible with the scale used), which was consistent with previous results.[24,53] The high-frequency loop remained quite unaffected, which means that the charge-transfer resistance was quite independent of the thickness of the thin layer both for the amplitude and the frequency. Until a frequency of 1 Hz, the diffusion loop also remained unchanged. However, below 1 Hz, an additional time constant was superimposed on the spherical diffusion. For a thin layer of 25 μm thick (L = 2.5), the impedance magnitude increases by 50−60%. The following Kramers−Kronig transforms[58,59] were used as a diagnostic tool to validate this low frequency behavior

$$\mathrm{Re}[Z(\omega)] = \mathrm{Re}[Z(\infty)] + \frac{2}{\pi}\int_{x=0}^{\infty} \frac{x\mathrm{Im}[Z(x)] - \omega\mathrm{Im}[Z(\omega)]}{x^2 - \omega^2}\mathrm{d}x \quad (13)$$

$$\mathrm{Im}[Z(\omega)] = \frac{2\omega}{\pi}\int_{x=0}^{\infty} \frac{\mathrm{Re}[Z(x)] - \mathrm{Re}[Z(\omega)]}{x^2 - \omega^2}\mathrm{d}x \quad (14)$$

Since Kramers−Kronig transforms are purely mathematical relationships, they provided an independent means by which to establish the formal consistency of experimental impedance data. For the experimental data presented in this work, a deviation of less than 2% was obtained for frequencies below 1 Hz.

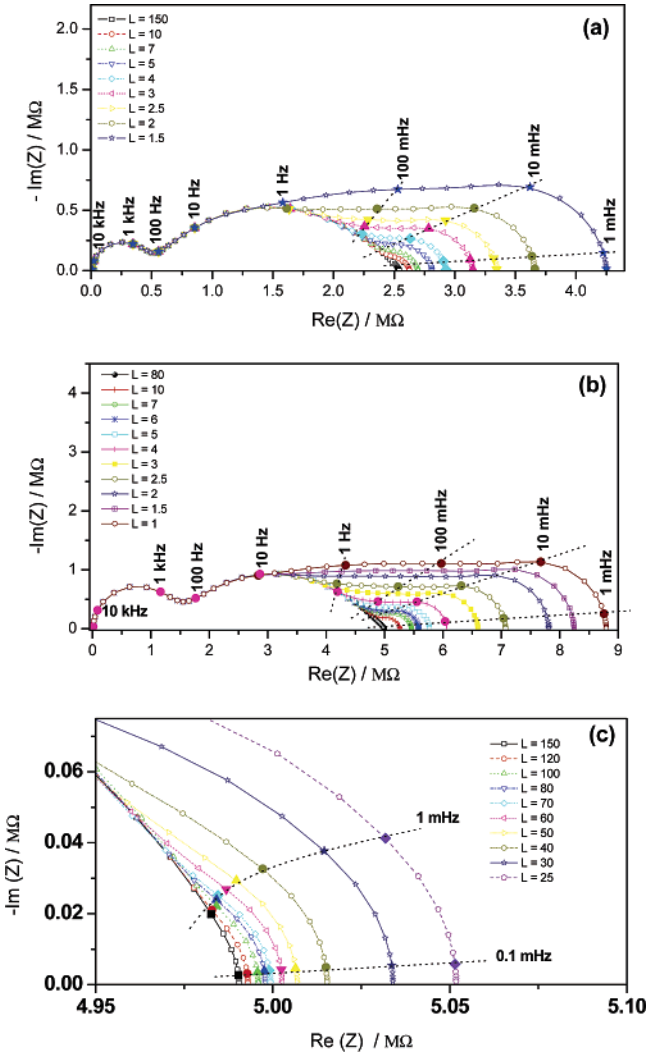

Figure 4. Calculated impedance diagrams of a microelectrode in a thin-layer cell with the dimensionless distance L as a parameter. (a) r = 10 μm; RG = 20; (b) r = 5 μm; RG = 40; (c) r = 5 μm; RG = 40; zoom in the low-frequency domain. For the three graphs: $k^0 = 2.5 \times 10^{-2}$ cm s^{-1}; $D = 6.5 \times 10^{-6}$ cm^2 s^{-1}; α = 0.5; C_{dl} = 60 μF cm^{-2}; C = 10 mM; and R_e = 10 kΩ.

Figure 4a shows impedance diagrams calculated for a 10 μm in diameter Pt-microelectrode with RG = 20 and with the dimensionless distance L as a parameter. The other parameters (see figure caption) are consistent with those determined from experimental results reported in Figure 2. For L = 150, which corresponds to a tip-to-substrate distance of 750 μm, the impedance diagram is similar to that obtained in the bulk solution. As the L parameter decreases, a further time constant appears at the low-frequency end. For L = 10, it shows up as a shoulder, but for L = 3, its magnitude significantly increases. Moreover, these calculated diagrams are in full agreement with the experimental results presented in Figure 3 for the range of impedance and frequency values. From the analysis of impedance data in the low-frequency range, the dependence of the low-frequency admittance on experimental parameter L was shown to be consistent with the dependence of the steady-state current of the SECM in the negative feedback mode.

For a thin layer with identical dimensions but with an UME that is 2 times smaller, which corresponds to r = 5 μm and RG

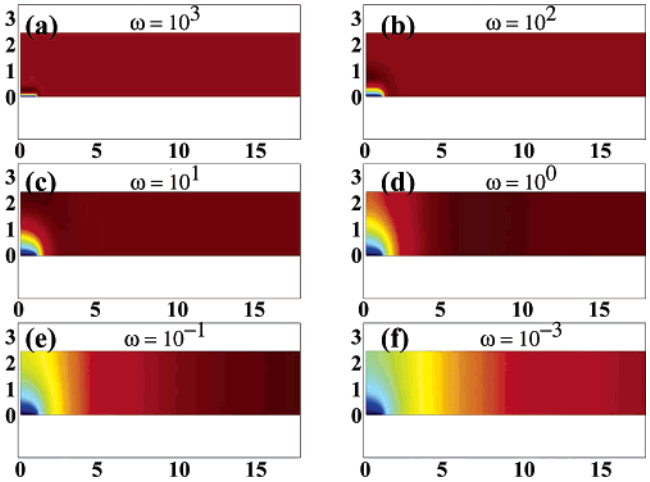

Figure 5. (a−f) Evolution of the concentration gradient in the thin-layer cell with angular frequency (in rad s^{-1}) as a parameter. $r = 10$ μm; $RG = 20$; $k^0 = 2.5 \times 10^{-2}$ cm s^{-1} ; $D = 6.5 \times 10^{-6}$ cm^2 s^{-1}; $\alpha = 0.5$; $C_{dl} = 60$ μF cm^{-2}; C = 10 mM; and $R_e = 10$ kΩ.

= 40, similar evolution of the impedance diagrams is observed (Figure 4b). However, the magnitude of the diffusion impedance is 2 times larger, which corresponds to the 2 times lower electrode radius. In contrast to measurements with conventional electrodes, the frequencies are scaled by the parameter (D/a^2), which was mentioned by Fleischmann et al.[5] In the low-frequency range (i.e., for $f < 1$ mHz) and for the large thin layer, the shape of the diagrams remains quite different from that predicted by Fleischmann et al.[5,15] Thus, the low-frequency tail of the impedance corresponds to a semicircle rather than a straight line with a slope of −45°. This assumption is also in accordance with Kramers−Kronig extrapolation in the low-frequency range. We ascribe this divergence of results to the fact that Fleischmann et al.[15] had to do some approximations to give a pseudo-analytical solution to the diffusion problem at a microelectrode. Nevertheless, from an experimental point of view and when the UME is in a bulk solution, this difference is of little significance because it appears in a frequency domain that is not easily investigatable.

These experimental and theoretical results suggest that two diffusion regimes have to be considered depending on the frequency range. This is illustrated by Figure 5, which shows the evolution of the concentration gradients in the thin-layer cell with angular frequency as a parameter. These figures correspond to the calculations presented in Figure 4a. In the high-frequency domain, that is for $\omega \geq 10$ rad s^{-1} (Figures 5a−c), the diffusion of the electroactive species can be related to a classical microdisk electrode behavior corresponding to spherical diffusion when the UME is far from any substrate. This is consistent with the attenuation of the concentration waves at higher frequencies in this frequency range. The low-frequency domain (for $\omega < 10$ rad s^{-1}, Figure 5d−f) exhibits a more complex response arising from a mixed diffusion behavior. First, the spherical diffusion is screened by the insulating substrate facing the microelectrode, and, second, the diffusion gradients show that concentration waves propagate in the thin layer through radial diffusion (from the right to the left in Figure 5e−f). This was confirmed by numerical simulations for a given L and with the dimensionless radius RG as a parameter (Figure 6). For $RG = 2$, no significant contribution of the radial diffusion is revealed in the impedance diagram, and the low-frequency limit is about 5 MΩ, whereas for $RG = 3$, a noticeable shoulder is shown in the low-frequency region (the polarization resistance

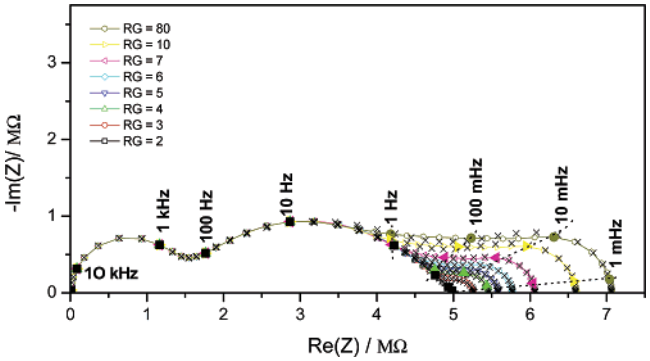

Figure 6. Calculated impedance diagrams of a microelectrode in a thin-layer cell with the dimensionless radius RG as a parameter. $r = 5$ μm; $k^0 = 2.5 \times 10^{-2}$ cm s^{-1}; $D = 6.5 \times 10^{-6}$ cm^2 s^{-1}; $\alpha = 0.5$; $C_{dl} = 60$ μF cm^{-2}; C = 10 mM; and $R_e = 10$ kΩ.

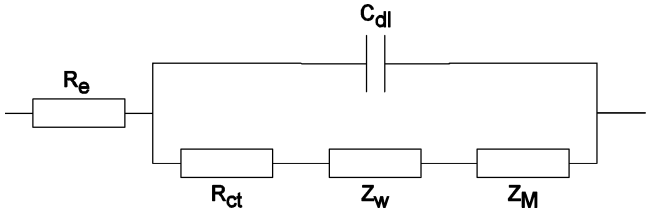

Figure 7. Equivalent circuit used for data analysis. R_e, electrolyte resistance; R_{ct}, charge-transfer resistance; Z_W, Cole−Davidson impedance; Z_M, Cole−Cole impedance.

reaches 5.3 MΩ), and it increases with RG. For instance, for a RG value of 80, the polarization resistance attains about 7.1 MΩ.

Discussion

In the first part of this paper, it was shown that the low-frequency part of the impedance of a microelectrode in a thin-layer cell is controlled by two types of transport: a spherical diffusion hindered by the insulating substrate and a radial diffusion through the thin layer. So far, the experimental data were compared to numerical calculations (from the physicochemical model determined by solving the Fick's law using finite element methods). These computations are not of common practice for the experimentalist; therefore, to characterize each process, we propose an equivalent circuit showing characteristic parameters.

Considering the previous results, the equivalent circuit presented in Figure 7 is proposed to take into account a simple electrochemical reaction occurring at a microelectrode in a thin-layer-cell configuration. It consists of a Randles-type equivalent circuit[10] in which the Warburg impedance is replaced by two contributions in series. The first one, Z_M, accounts for the spherical diffusion and is defined as a Cole−Cole impedance

$$Z_M(\omega) = \frac{R_M}{1 + (j\omega\tau_M)^{\alpha_M}} \tag{15}$$

and the second one, Z_W, accounts for the low-frequency contribution. A Cole−Davidson-type impedance was used

$$Z_W(\omega) = \frac{R_W}{(1 + j\omega\tau_W)^{\alpha_W}} \tag{16}$$

It is noticeable that a Cole−Davidson relaxation with $\alpha_W = 0.5$ gives a diagram very close to the usual linear diffusion with

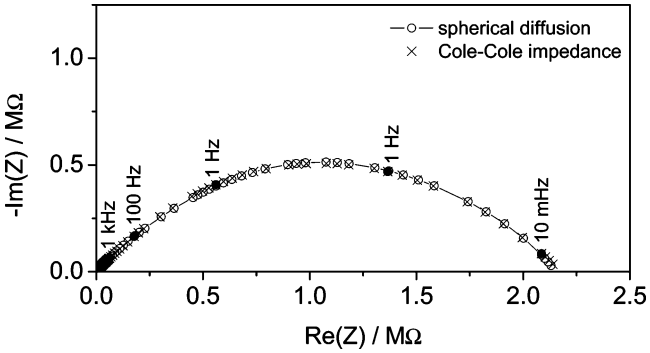

Figure 8. Spherical diffusion calculated by FEM for a microelectrode in a solution bulk. $r = 10$ μm; $RG = 20$; $D = 6.5 \times 10^{-6}$ cm^2 s^{-1} (circle) and nonlinear fit with a Cole−Cole impedance (cross).

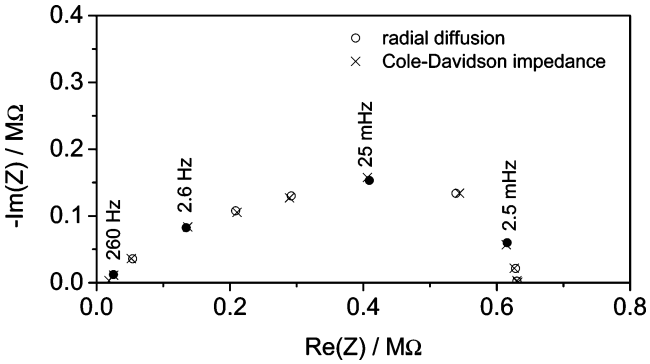

Figure 9. Radial diffusion calculated by FEM for a microelectrode in a thin-layer-cell configuration. $r = 10$ μm; $RG = 20$; $L = 2.5$; $D = 6.5 \times 10^{-6}$ cm^2 s^{-1} (circle) and nonlinear fit with a Cole−Davidson impedance (cross).

a fixed diffusion layer thickness, δ, often modeled by

$$Z_\delta(\omega) = R_D \frac{\tanh(\sqrt{j\omega\tau_d})}{\sqrt{j\omega\tau_d}} \qquad (17)$$

where $\tau_d = \delta^2/D$, and R_D is a scaling coefficient.

Figure 8 (circle) shows a typical impedance diagram for the spherical diffusion calculated for a 10-μm-diameter microelectrode and a diffusion coefficient of 6.5×10^{-6} cm^2 s^{-1}. From a nonlinear regression with the Simplex algorithm, it is shown that the Cole−Cole formula allows the spherical diffusion to be calculated with an error as low as 0.2%. In that case, the fitted parameters were $R_M = 2.03 \times 10^6$ Ω, $\alpha_M = 0.52$, and a characteristic frequency of 2.2 Hz was determined. Similarly, Figure 9 (circle) shows a typical impedance diagram for the radial diffusion. It was calculated for a 10-μm-diameter microelectrode, $L = 2.5$ for the thin-layer thickness, and a diffusion coefficient of 6.5×10^{-6} cm^2 s^{-1}. Qualitatively, the shape of the diagrams and the time constant are in good agreement with the low-frequency time-constant observed on the experimental results. Moreover, using a nonlinear regression with the Simplex algorithm, it is shown that the Cole−Davidson formula allows the radial diffusion to be simulated with an error as low as 0.7%, which allows the parameters $R_W = 5.11 \times 10^5$ Ω, $\alpha_W = 0.34$, and the characteristic frequency 2.3×10^{-2} Hz to be determined.

From these results, it is concluded that the equivalent circuit proposed in Figure 7 for describing the diffusion at a microelectrode in a thin-layer cell is suitable. When the electrolyte resistance, the charge-transfer resistance, and the double-layer capacitance are taken into account, the overall impedance is

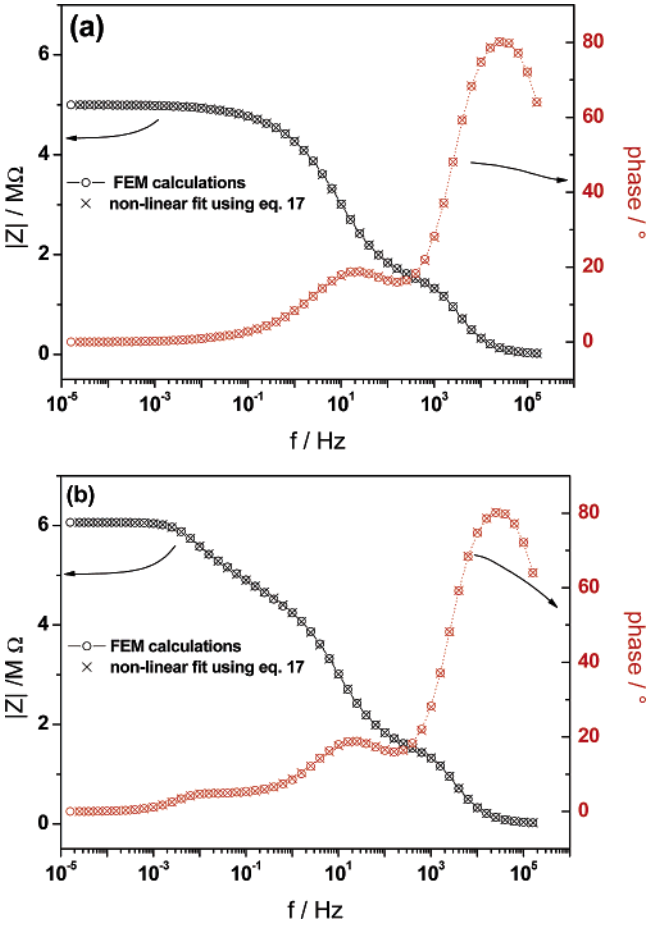

Figure 10. FEM simulations (circle) and nonlinear fit (cross) of impedance diagrams in a Bode representation for a microelectrode in a thin-layer cell for (a) $L = 80$ and (b) $L = 3.6$. For both figures, the other parameters are the following: $r = 5$ μm; $RG = 50$; $k^0 = 2.5 \times 10^{-2}$ cm s^{-1}; $D = 6.5 \times 10^{-6}$ cm^2 s^{-1}; $\alpha = 0.5$; $C_{dl} = 60$ μF cm^{-2}; $C = 10$ mM; and $R_e = 10$ kΩ.

thus given by the relationship

$$Z(\omega) = R_e + \frac{R_{ct} + Z_M + Z_W}{1 + jC_{dl}\omega\,(R_{ct} + Z_M + Z_W)} \qquad (18)$$

Let us now consider the FEM simulations (Figure 10, open circle) of impedance diagrams in a Bode representation for a microelectrode in a thin-layer cell. Calculations were performed for two different thicknesses of the thin layer in which $L = 80$ (Figure 10a) and $L = 3.6$ (Figure 10b). The other parameters were the same for the two figures and are given in the figure caption. The simplest situation arises when the microelectrode was far from the substrate (Figure 10a), that is, when the diffusion at the UME can be described by spherical diffusion. The use of eq 18 in combination with a nonlinear regression with the Simplex algorithm allowed both the modulus and the phase shift to be perfectly fitted with respect to the frequency. When the microelectrode was close to the insulating substrate (open circle in Figure 10b), both spherical and radial contributions of the diffusion were evidenced especially in the low-frequency range. The fit of the impedance diagram using eq 18 (cross) was seen to be very good in the whole frequency range (the discrepancy was estimated at 0.4% from the fitting procedure). Although the equivalent circuit presented in Figure 7 provided an excellent fit to the data, a divergence of up to approximately 4% was observed for the fitting of larger values of RG, as shown for $RG = 80$ in Figure 6. Similar observations

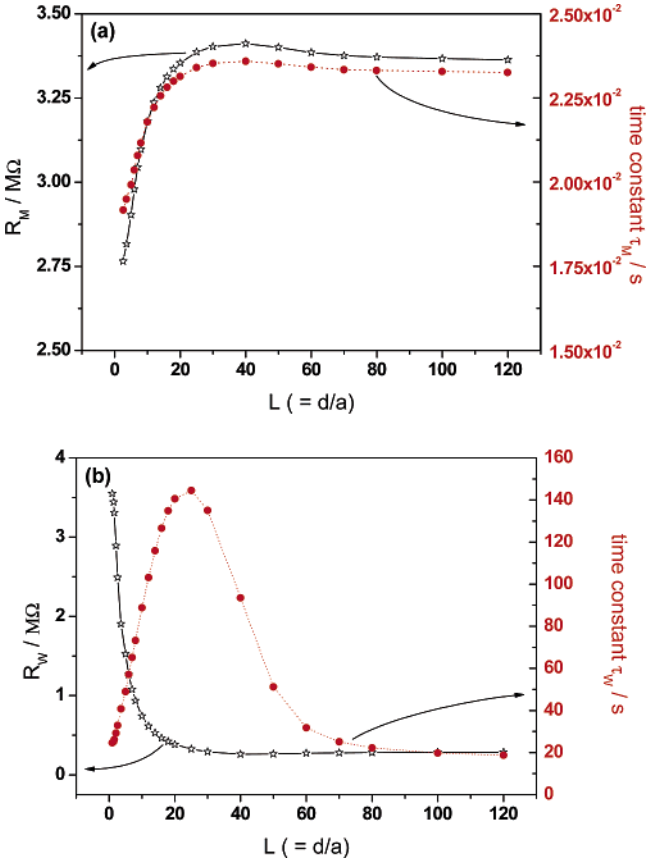

Figure 11. Evolution of the impedance parameters of eq 18 with a nonlinear fit (Simplex algorithm) for calculated impedance diagrams of a microelectrode in a thin-layer cell with the dimensionless distance L as a parameter. (a) R_M and τ_M and (b) R_W and τ_W. For both figures, the other parameters are the following: $r = 5\ \mu$m; $RG = 50$; $k^0 = 2.5 \times 10^{-2}$ cm s^{-1}; $D = 6.5 \times 10^{-6}$ cm^2 s^{-1}; $\alpha = 0.5$; $C_{dl} = 60\ \mu$F cm^{-2}; $C = 10$ mM; and $R_e = 10$ kΩ.

were made when performing calculations with the thin-layer thickness, L, as a parameter (data not shown). The fit of the data with the help of the equivalent circuit presented in Figure 7 was achieved with a good accuracy (lower than 1%) for $L > 1.5$. For smaller L values, a significant deviation between the fit and the FEM calculations was obtained. Thus, careful attention was paid to the meshing with the FEM algorithm. Triangular finite elements were used with a finer mesh over the microdisk and around geometric singularities than in the bulk domain. The mesh away from the disk was kept as fine as possible considering the limitation of the computer memory; however, no improvement could be obtained and the divergence remained constant. By taking into account all of the calculations achieved for this work, it was found empirically that if the ratio of RG/L was lower than 60, the deviation between the fit and the FEM calculations remained lower than 2%.

The fitting of the FEM calculations performed with L as a parameter provides the evolution of R_M and τ_M (from the Cole−Cole impedance) shown in Figure 11a and R_W and τ_W (from Cole−Davidson impedance) shown in Figure 11b. For the Cole−Cole type component, both R_M and τ_M exhibit the same variations. They slowly increase for the decreasing value of L from $L = 120$ to $L = 30$ then decrease until $L = 2$. The main variations of these parameters are observed for $2 \le L \le 30$. This is consistent with the previous observations. The variations of R_W and τ_W are different. First, it should be noted that even for the larger values of L, R_W is not equal to zero and remains constant for $L > 30$. As a result, for a microelectrode immersed in bulk solution, a radial contribution (only visible in the low-frequency range) takes place in the diffusional process. For $L < 30$, R_W rises dramatically as L decreases. Second, τ_W variations are unexpected, since the time constant is at a peak for $L = 30$. Moreover, τ_W increases on the entire domain on which R_W has a constant value. It must be emphasized, however, that this behavior cannot be interpreted as a miscalculation. Indeed, the impedance diagrams calculated for $25 \le L \le 160$, which are reported in Figure 4c, clearly show that for large L values, a shoulder in the low-frequency range is still evidenced. Thus, these parameter variations indicate that two regions can be distinguished:

(i) For large L values, the key parameter is the time constant, τ_W, which increases, whereas all the other parameters remain quite unchanged.

(ii) For $L < 30$, when L decreases, R_M and τ_M decrease. Simultaneously, the contribution of the radial diffusion increases.

Conclusion

We have shown in this work that it is possible to perform electrochemical impedance spectroscopy on a microdisk electrode in a thin-layer-cell geometry. This configuration was achieved using a scanning electrochemical microscope to control the thin-layer thickness.

From both experimental data and numerical calculations using a physicochemical model, it was shown that in addition to the spherical diffusion the radial contribution of the diffusion evidenced in the low-frequency range cannot be neglected in thin-layer-cell configuration, and it depends on both thin-layer thickness and diameter.

An equivalent circuit for the impedance measurements on a microelectrode in the thin-layer-cell configuration was proposed to characterize the two transport processes in a simpler manner. It was based on a Randles-type circuit in which the Warburg component was replaced by a Cole−Cole impedance and a Cole−Davidson impedance. The first one accounted for the spherical diffusion, whereas the second one was introduced to describe the radial diffusion. This circuit allowed a suitable fit of the data (within a maximum error of 2%) for $RG/L < 60$.

Nomenclature

a = radius of the microelectrode.
c = concentration of the electroactive species.
c^∞ = bulk concentration of the electroactive species.
C_{dl} = double-layer capacitance.
d = tip-to-substrate distance.
D_i = diffusion coefficient of the species i.
f = frequency.
F = Faraday constant.
i_0 = exchanged current density.
I = current.
I_{Norm} = normalized current ($I_{Norm} = I/I_\infty$).
I_∞ = steady-state current at a disk microelectrode ($I_\infty = 4nFDCa$).
Im(Z) = imaginary part of the complex number Z.
j = complex number ($j^2 = -1$).
k_b = kinetic constant of the reduction step.
k_f = kinetic constant of the oxidation step.
k_0 = standard rate constant of the electrochemical reaction.
L = normalized tip-to-substrate distance ($L = d/a$).
n = number of electrons involved in the electrochemical reaction.
R = gas constant.
R_e = electrolyte resistance.

R_M = resistance of the Cole−Cole impedance.
R_W = resistance of the Cole−Davidson impedance.
r_g = total radius of the microelectrode (wire and insulating material).
R_{ct} = charge-transfer resistance.
Re*(Z)* = real part of the complex number *Z*.
RG = dimensionless sheath radius ($RG = r_g/a$).
t = time.
T = temperature.
v_z = approach rate.
Z = impedance.
Z_d = diffusion impedance.
Z_M = Cole−Cole impedance.
Z_W = Cole−Davidson impedance.
α = charge-transfer coefficient.
α_M = frequency-independent number ($0 \leq \alpha_M \leq 1$) of the Cole−Cole impedance.
α_W = frequency-independent number ($0 \leq \alpha_W \leq 1$) of the Cole−Davidson impedance.
β = tilt angle between the tip and the substrate.
δ = diffusion layer thickness.
ΔE = normalized potential perturbation at the electrode surface.
$\Delta\tilde{E}(\omega)$ = potential (complex number).
$\Delta\tilde{I}(\omega)$ = current (complex number).
Φ_4 = tabulated function (in ref 5).

References and Notes

(1) Dayton, M. A.; Brown, J. C.; Stutts, K. J.; Wightman, R. M. *Anal. Chem.* **1980**, *52*, 946−950.
(2) Dayton, M. A.; Ewing, A. G.; Wightman, R. M. *Anal. Chem.* **1980**, *52*, 2392−2396.
(3) Bond, A. M.; Fleischmann, M.; Robinson, J. *J. Electroanal. Chem. Interfacial Electrochem.* **1984**, *172*, 11−25.
(4) Bond, A. M.; Fleischmann, M.; Robinson, J. *J. Electroanal. Chem. Interfacial Electrochem.* **1984**, *168*, 299−312.
(5) Fleischmann, M.; Pons, S.; Rolinson, D. R.; Schmidt, P. P. *Ultramicroelectrodes*; Datatech Systems, Inc.: Morganton, NC, 1987.
(6) Andrieux, C. P.; Hapiot, P.; Saveant, J. M. *Chem. Rev.* **1990**, *90*, 723−738.
(7) Amatore, C. In *Physical Electrochemistry. Principles, methods, and applications*; Rubinstein, I., Ed.; Marcel Dekker: New York, 1995.
(8) Forster, R. J. *Chem. Soc. Rev.* **1994**, *23*, 289−297.
(9) Bard, A. J.; Faulkner, L. R. *Electrochemical Methods: Fundamentals and Applications*, 2nd ed.; Wiley−VCH: New York, 2001.
(10) Gabrielli, C. In *Physical Electrochemistry. Principles, methods, and applications*; Rubinstein, I., Ed.; Marcel Dekker: New York, 1995.
(11) Macdonald, D. D. *Electrochim. Acta* **2006**, *51*, 1376−1388.
(12) Thomas, A. B.; Brodd, R. J. *J. Phys. Chem.* **1964**, *68*, 3363−3367.
(13) Bezegh, A.; Janata, J. *J. Electroanal. Chem. Interfacial Electrochem.* **1986**, *215*, 139−149.
(14) Baranski, A. S. *J. Electrochem. Soc.* **1986**, *133*, 93−97.
(15) Fleischmann, M.; Pons, S.; Daschbach, J. *J. Electroanal. Chem.* **1991**, *317*, 1−26.
(16) Bruce, P. G.; Lisowska-Oleksiak, A.; Los, P.; Vincent, C. A. *J. Electroanal. Chem.* **1994**, *367*, 279−283.
(17) Mcnaughtan, A.; Ansell, R. O.; Pugh, J. R. *Meas. Sci. Technol.* **1994**, *5*, 789−792.
(18) Baranski, A. S.; Szulborska, A. *Electrochim. Acta* **1996**, *41*, 985−991.
(19) Baranski, A. S.; Krogulec, T.; Nelson, L. J.; Norouzi, P. *Anal. Chem.* **1998**, *70*, 2895−2901.
(20) Rodewald, S.; Fleig, J.; Maier, J. *J. Eur. Ceram. Soc.* **1999**, *19*, 797−801.
(21) Ferrigno, R.; Girault, H. H. *J. Electroanal. Chem.* **2000**, *492*, 1−6.
(22) Aoki, K.; Tokida, A. *Electrochim. Acta* **2000**, *45*, 3483−3488.
(23) Cachet, C.; Cachet, H.; Jousseaume, B.; Toupance, T.; Vivier, V. *Electrochim. Acta* **2002**, *47*, 1385−1394.
(24) Gabrielli, C.; Huet, F.; Keddam, M.; Rousseau, P.; Vivier, V. *J. Phys. Chem. B* **2004**, *108*, 11620−11626.
(25) Pernkopf, W.; Sagl, M.; Fafilek, G.; Besenhard, J. O.; Kronberger, H.; Nauer, G. E. *Solid State Ionics* **2005**, *176*, 2031−2036.
(26) Bai, X.; Dexter, S. C.; Luther, G. W. *Electrochim. Acta* **2006**, *51*, 1524−1533.
(27) Koehler, S.; Bund, A. *J. Phys. Chem. B* **2006**, *3*, 1485−1489.
(28) Serghini-Idrissi, M.; Bernard, M. C.; Harrif, F. Z.; Joiret, S.; Rahmouni, K.; Srhiri, A.; Takenouti, H.; Vivier, V.; Ziani, M. *Electrochim. Acta* **2005**, *50*, 4699−4709.
(29) Zou, F.; Thierry, D.; Isaacs, H. S. *J. Electrochem. Soc.* **1997**, *144*, 1957−1965.
(30) Alpuche-Aviles, M. A.; Wipf, D. O. *Anal. Chem.* **2001**, *73*, 4873−4881.
(31) Gabrielli, C.; Ostermann, E.; Perrot, H.; Vivier, V.; Beitone, L.; Mace, C. *Electrochem. Commun.* **2005**, *7*, 962−968.
(32) Etienne, M.; Schulte, A.; Schuhmann, W. *Electrochem. Commun.* **2004**, *6*, 288−293.
(33) Katemann, B. B.; Gonzalez Inchauspe, C.; Castro, P. A.; Schulte, A.; Calvo, E. J.; Schuhmann, W. *Electrochim. Acta* **2003**, *48*, 1115−1121.
(34) Ervin, E. N.; White, H. S.; Baker, L. A. *Anal. Chem.* **2005**, *77*, 5564−5569.
(35) Amatore, C.; Svir, I. *J. Electroanal. Chem.* **2003**, *557*, 75−90.
(36) Gavaghan, D. J. *J. Electroanal. Chem.* **1998**, *456*, 25−35.
(37) Gavaghan, D. J. *J. Electroanal. Chem.* **1998**, *456*, 13−23.
(38) Gavaghan, D. J. *J. Electroanal. Chem.* **1998**, *456*, 1−12.
(39) Gillow, K.; Gavaghan, D. J.; Sueli, E. *J. Electroanal. Chem.* **2006**, *587*, 1−17.
(40) Ferrigno, R.; Brevet, P. F.; Girault, H. H. *Electrochim. Acta* **1997**, *42*, 1895−1903.
(41) Lee, H. J.; Beriet, C.; Ferrigno, R.; Girault, H. H. *J. Electroanal. Chem.* **2001**, *502*, 138−145.
(42) Hubbard, A. T.; Anson, F. C. In *Electroanalytical Chemistry*; Bard, A. J., Ed.; Marcel Dekker: New York, 1970.
(43) Hubbard, A. T.; Anson, F. C. *Anal. Chem.* **1964**, *36*, 723−726.
(44) Hubbard, A. T.; Anson, F. C. *Anal. Chem.* **1966**, *38*, 58−61.
(45) Engstrom, R. C.; Weber, M.; Wunder, D. J.; Burgess, R.; Winquist, S. *Anal. Chem.* **1986**, *58*, 844−848.
(46) Engstrom, R. C.; Meaney, T.; Tople, R.; Wightman, R. M. *Anal. Chem.* **1987**, *59*, 2005−2010.
(47) Bard, A. J.; Fan, F.-R. F.; Kwak, J.; Lev, O. *Anal. Chem.* **1989**, *61*, 132−138.
(48) Mandler, D.; Bard, A. J. *J. Electrochem. Soc.* **1989**, *136*, 3143−3144.
(49) Wipf, D. O.; Bard, A. J.; Tallman, D. E. *Anal. Chem.* **1993**, *65*, 1373−1377.
(50) Gabrielli, C.; Huet, F.; Keddam, M.; Rousseau, P.; Vivier, V. *Electrochem. Solid-State Lett.* **2003**, *6*, E23−E26.
(51) Gabrielli, C.; Joiret, S.; Keddam, M.; Perrot, H.; Portail, N.; Rousseau, P.; Vivier, V. *J. Electrochem. Soc.* **2006**, *153*, B68−B74.
(52) Arca, M.; Bard, A. J.; Horrocks, B. R.; Richards, T. C.; Treichel, D. A. *Analyst (Cambridge, U.K.)* **1994**, *119*, 719−726.
(53) Horrocks, B. R.; Mirkin, M. V.; Pierce, D. T.; Bard, A. J.; Nagy, G.; Toth, K. *Anal. Chem.* **1993**, *65*, 1213−1224.
(54) Newman, J. *J. Electrochem. Soc.* **1966**, *113*, 501−502.
(55) Iwasita, T.; Schmickler, W.; Herrmann, J.; Vogel, U. *J. Electrochem. Soc.* **1983**, *130*, 2026−2032.
(56) Huang, W.; McCreery, R. *J. Electroanal. Chem.* **1992**, *326*, 1−12.
(57) Deslouis, C. Tribollet, B.; Viet, L. *Electrochim. Acta* **1980**, *25*, 1027−1032.
(58) Gabrielli, C.; Keddam, M.; Takenouti, H. *ASTM Spec. Tech. Publ.* **1993**, *STP 1188*, 140−153.
(59) Dougherty, B. J.; Smedley, S. I. *ASTM Spec. Tech. Publ.* **1993**, *STP 1188*, 154−170.